CAPACITIVE TOMOGRAPHY FOR THE LOCATION OF PLASTIC PIPE

FINAL TECHNICAL REPORT

Principal Investigator: Brian J. Huber
Project Manager: Christopher J. Ziolkowski

847-768-0549, chris.ziolkowski@gastechnology.org

Report Issue Date: December 30, 2003

DOE Contract #: DE-FC26-01NT41161

Submitted by

Gas Technology Institute
1700 South Mount Prospect Road
Des Plaines, Illinois 60018

GTI Project Number: 61140

Submitted to

NETL AAD Document Control Bldg. 921
U.S. Department of Energy
National Energy Technology Laboratory
P.O. Box 10940
Pittsburgh, PA 15236-0940

DOE Project Officer
Anthony Zammerilli

DISCLAIMER

RESEARCH SUMMARY

Title: Capacitive Tomography for the Detection of Plastic Pipe

Contractor(s): Gas Technology Institute
Contract Number: DE-FC26-01NT41161

Principal Investigator(s): Christopher Ziolkowski
Brian Huber

Report Type: Final Report
Report Period: October 2001 – September 2003

Objective:
The objective of this program was to develop and test a system that would detect and image buried plastic and ceramic pipe. The system is designed to detect variations in the electric permeability of soil corresponding to the presence of a buried plastic pipe. The Gas Technology Institute (GTI) proposed to develop a compact and inexpensive capacitive tomography-imaging sensor that can be placed on the ground to image objects embedded in the soil. The system provides a coarse image, which allows the operator to identify a buried object's location both horizontally and vertically.

Technical perspective:
Throughout the utility industry, there is high interest in subsurface imaging of plastic, ceramic, and metallic objects because of the cost, reliability, and safety benefits available in avoiding impacts with the existing infrastructure and in reducing inappropriate excavations. A compact, low-cost sensor that can image objects through soil could be applied to multiple operations and will produce a number of cost savings for the gas industry. Ground Probing Radar has only partially fulfilled this need. GPR has difficulty in wet or mineralized soils and also requires a well-trained operator to interpret the GPR results even in optimal conditions.

Technical Approach:
The sensor takes the form of a flat array of electrodes that is fabricated using printed circuit board techniques. The image resolution is proportional to the number and spacing of the electrodes in the array. An excitation signal is injected into the soil at several frequencies in the 100kHz to 200kHz range. The complex impedance between adjacent electrodes provides the image data. An electronics package amplifies and scans the signals from the various electrodes. The sensor signals are then collected on a PC via a data acquisition board. The PC data is displayed in a Graphical User Interface written in National Instruments LabVIEW.

Results:
Over the course of the project several 24-inch square printed circuit board sensor arrays were fabricated. A four-element array was constructed first and was readily able to detect a 4" plastic pipe buried in 4' of soil. A 16-element array was then produced along with electronics for interfacing the signals from the sensor array to the PC. This second generation improved signal strength by as much as a factor of 100. Runs of 2", 4" and 6" PE pipe were installed on GTI property as test targets. The 16-element array readily detects PE pipe in up to 5' of wet soil.

A simple imaging protocol was implemented. This consisted of 16 square elements arranged on a grid on the PC screen corresponding to the elements in the sensor array. The elements would lighten or darken according to the strength of the received signal directly under the sensor element. Looking at the grid one can get a coarse "silhouette" type image of objects in the soil beneath the sensor array.

A two-wheeled cart has been constructed with the 16-element sensor board mounted to the cart. An operator can easily push the cart over an area of interest to perform imaging. This arrangement was publicly demonstrated at the Underground Focus Live trade show this summer. This show allowed favorable side-by-side comparisons of CT with several GPR imaging systems. CT provides a much more intuitive image of subsurface objects than GPR.

A 64-element multilayer sensor board with surface mount components has been constructed. This sensor board will increase the image resolution by a factor of 4. The use of surface mount components should eliminate sensor element cable loading and other parasitic effects.

Project Implication:
CT imaging provides an alternative subsurface imaging to GPR. It has several distinct advantages. CT is not hindered by wet soils. The CT electronics can be produced at lower cost than that for GPR. The image produced by CT is easy to interpret and does not require extensive operator training. GTI will seek funding to take the CT from proof-of-concept to a prototype more suitable for commercial production.

ABSTRACT

Throughout the utility industry, there is high interest in subsurface imaging of plastic, ceramic, and metallic objects because of the cost, reliability, and safety benefits available in avoiding impacts with the existing infrastructure and in reducing inappropriate excavations. Industry interest in locating plastic pipe has resulted in funding available for the development of technologies that enable this imaging. Gas Technology Institute (GTI) proposes to develop a compact and inexpensive capacitive tomography imaging sensor that takes the form of a flat plate or flexible mat that can be placed on the ground to image objects embedded in the soil.

A compact, low-cost sensor that can image objects through soil could be applied to multiple operations and will produce a number of cost savings for the gas industry. In a stand-alone mode, it could be used to survey an area prior to excavation. The technology would improve the accuracy and reliability of any operation that involves excavation by locating or avoiding buried objects. An accurate subsurface image of an area will enable less costly keyhole excavations and other cost-saving techniques.

Ground penetrating radar (GPR) has been applied to this area with limited success. Radar requires a high-frequency carrier to be injected into the soil: the higher the frequency, the greater the image resolution. Unfortunately, high-frequency radio waves are more readily absorbed by soil. Also, high-frequency operation raises the cost of the associated electronics. By contrast, the capacitive tomography sensor uses low frequencies with a multiple-element antenna to obtain good resolution. Low-frequency operation lowers the cost of the associated electronics while improving depth of penetration.

The objective of this project is to combine several existing techniques in the area of capacitive sensing to quickly produce a demonstrable prototype. The sensor itself will take the form of a flat array of electrodes that can be inexpensively fabricated using printed circuit board techniques. The image resolution is proportional to the number and spacing of the electrodes in the array. Measuring the complex impedance between adjacent electrodes at multiple frequencies forms the image. Simple location of plastic pipe with a two-electrode array has already been demonstrated.

Thus far, 4-element and 16-element sensor arrays have been fabricated on 24” by 24” printed circuit boards and tested. The sensor arrays have been tested with buried plastic piping at GTI both in soil boxes and an outdoor facility. Sensitivity to the presence of plastic pipe in soil has been demonstrated with 2”, 4”, and 6” diameter pipes at depths greater than 4 feet. This sensitivity is unaffected by soil moisture conditions. A 64-element array is currently being fabricated to provide greater spatial resolution of buried objects.

TABLE OF CONTENTS

LIST OF GRAPHICAL MATERIALS

EXECUTIVE SUMMARY

Excavation is an inherently expensive and risky operation that utilities seek to minimize. The cost of an excavation can range from $500 to $5,000 depending on the size and location. Extremely small (or, keyhole) excavations require very accurate targeting to be effective. Full-size excavations need to span the desired subsurface features in the first attempt, and rework of any type of excavation is expensive and disruptive. Less easily quantified are the losses incurred during dig-ins or impacts with the existing buried infrastructure resulting from faulty location data. These incidents require the mobilization of whatever resources are required to effect immediate repair, disrupting other operations. A release of gas, water, or a breach of an electrical main can severely affect the safety of workers and the public.

Directional boring is another technology that is being used to reduce the number of excavations. In this operation, a boring tool is used to create a pilot tunnel between two widely spaced pits. The boring tool is then pulled back to the entry pit drawing new plastic pipe with it. There have been instances of plastic pipe inadvertently intersecting clay sewer lines during the directional boring operation. When attempts were made to clear the blocked sewer line, the plastic gas pipe was breached, filling the sewer system with gas. There is at least one documented instance of an explosion caused by this situation. This hazardous situation could have been prevented with better subsurface imaging. Specifically, there is a need to accurately image non-metallic sewer lines as well as the plastic pipe.

In light of the consequences of faulty location data, the gas industry would be quick to adopt a subsurface imaging technology that meets their criteria. GTI industry advisors have identified this area as a high priority as demonstrated by the efforts expended on it to date. Current subsurface technologies to image non-metallic pipes, such as GPR and acoustic locators, are in limited use. A better technology would have excellent prospects for commercial deployment.

Because of its access to gas industry research, GTI is familiar with the merits and shortcomings of the various methods of subsurface imaging that have been attempted. The proposed capacitive tomography-imaging sensor directly addresses several deficiencies of the currently available technologies. The capacitive tomography technique is sensitive to the presence of plastic and ceramic piping materials. In addition, the thin-film nature of the sensor makes it adaptable to multiple applications. Also, capacitive tomography will give greater depth of penetration at a lower cost than ground-penetrating radar.

INTRODUCTION

Throughout the utility industry, there is high interest in subsurface imaging of plastic, ceramic, and metallic objects because of the cost, reliability, and safety benefits available in avoiding impacts with the existing infrastructure and in reducing inappropriate excavations. Industry interest in locating plastic pipe has resulted in funding available for the development of technologies that enable this imaging. Gas Technology Institute (GTI) is developing a compact and inexpensive capacitive tomography imaging sensor that takes the form of a flat plate or flexible mat that can be placed on the ground to image objects embedded in the soil.

A compact, low-cost sensor that can image objects through soil could be applied to multiple operations and will produce a number of cost savings for the gas industry. In a stand-alone mode, it could be used to survey an area prior to excavation. The technology would improve the accuracy and reliability of any operation that involves excavation by locating or avoiding buried objects. An accurate subsurface image of an area will enable less costly keyhole excavations and other cost-saving techniques.

Ground penetrating radar (GPR) has been applied to this area with limited success. Radar requires a high-frequency carrier to be injected into the soil: the higher the frequency, the greater the image resolution. Unfortunately, high-frequency radio waves are more readily absorbed by soil. Also, high-frequency operation raises the cost of the associated electronics. By contrast, the capacitive tomography sensor uses low frequencies with a multiple-element antenna to obtain good resolution. Low-frequency operation lowers the cost of the associated electronics while improving depth of penetration.

The sensor itself has taken the form of a flat array of electrodes that can be inexpensively fabricated using printed circuit board techniques. The image resolution is proportional to the number and spacing of the electrodes in the array. Measuring the complex impedance between adjacent electrodes at multiple frequencies forms the image. Simple location of plastic pipe with a two-electrode array has already been demonstrated.

Because of its access to gas industry research, GTI is familiar with the merits and shortcomings of the various methods of subsurface imaging that have been attempted. The capacitive tomography-imaging sensor directly addresses several deficiencies of the currently available technologies. The capacitive tomography technique is sensitive to the presence of plastic and ceramic piping materials. In addition, the thin-film nature of the sensor makes it adaptable to multiple applications. Also, capacitive tomography gives greater depth of penetration at a lower cost than ground-penetrating radar.

The capacitive tomographic technique performs a low-frequency impedance measurement using a multiple-element antenna array. The impedance of the soil and inclusions is sensitive to the dielectric properties of the inclusions as well as their conductivities. Thus, the technique is sensitive to plastic and metallic objects both.

Capacitive tomography is the detection of the structural details of an object by monitoring changes in an electric field produced by that object. The electric field most often will be produced by an arrangement of capacitive elements. The CT sensor array consists of a number of electric field producing and electric field detection elements configured in a planar array. The field producing elements or transmission elements is driven by a 100-400 kHz signal. The planar array is placed directly on or proximate to the surface of the ground. The system is configured to detect natural gas pipeline structures, in particular those that are composed of non-metallic materials, such as plastic or ceramic pipe.

A capacitor is a physical device that stores energy in the form of an electric field. The electric field that stores this energy may be time dependant or static. The type of physical structures that may be used to generate the electric field is typically an arrangement of metallic plates.

Strictly speaking capacitive tomography should be defined as the detection, sensing, or imaging of physical structures by the detection and analysis of variations or perturbations in the electric field parameters. These changes in the electric field parameters results from changes in the electrical permitivities of the physical structures that reside in the physical space that is being sensed. Thus there should be negligible self-interference of the electromagnetic field brought about by the physical dimensions of the capacitor elements that is generating the electrical fields. This would imply that the size of the capacitor plates and the distances between the plates and the structures to be detected would be very small compared to the wavelength of the electric fields.

In order to develop and test the concept of capacitive tomography, sensor arrays and support electronics were constructed. The spacing of the sensor array elements sets the resolution of the system, allowing the use of long wavelengths. In fact, any desired wavelength can be used, allowing the technique to be tuned to a particular soil. Low-frequency operation simplifies the signal processing requirements. The measurement of the soil impedance at a particular frequency can be done with simple circuitry.

Radar, by contrast, is a time-of-flight method requiring measurement of the interval between sending a radio pulse into the soil and the reflected echo from a buried object. This

requires expensive, high-speed electronics. The expense of the electronics limits Ground Penetrating Radar (GPR) to operation at one or two fixed frequencies. GPR uses short-wavelength radiation to achieve good position resolution and imaging. These short wavelengths are attenuated more severely by the soil than are long wavelengths.

The motivating concept for the CT sensor is shown in the following diagram. Sensor elements are driven by discrete capacitor C1 and C2 from signal source Vg(t). Electric field lines travel from the sensor plates 1 and sensor plate 2 to the ground frame on the perimeter of the figure. Vo(t) is the sensor output.

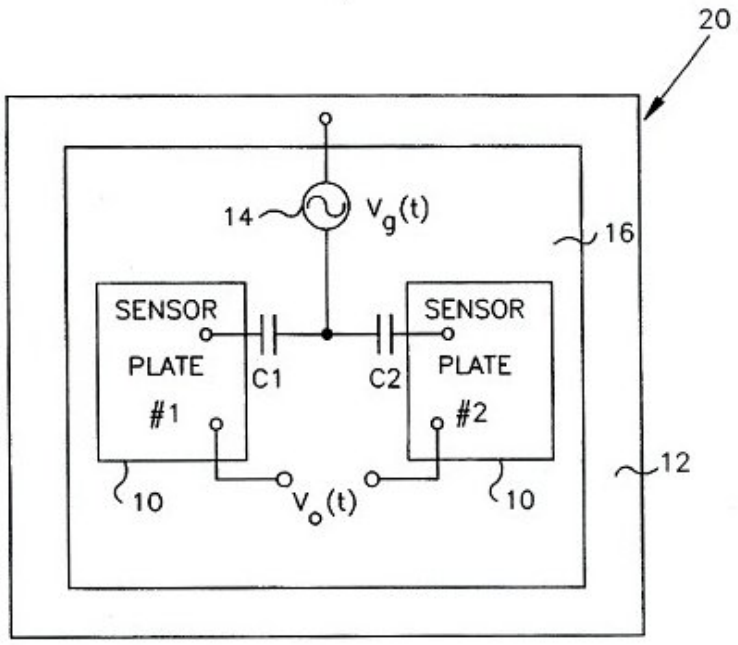

Figure 1. Patent Diagram from "Buried Pipe Locator Utilizing a Change in Ground Capacitance"

Four Element Sensor Array

The first prototype sensor array was fabricated in February of 2002. The sensor array is shown in figure 2. It was fabricated using conventional printed circuit board technology. It was approximately 24 inches square with 4, 8 inch by 8 inch sensor elements. The outer perimeter of the sensor array functioned as the return path for the electric field lines emanating from the sensor elements. It is the disruption of the electric field lines between the sensor elements and the perimeter element that creates the sensing capabilities of the array. The sensor array was initially resistor driven with sensor output acquired through an instrumentation amplifier followed by a bench top lock in amplifier. The bench lock in amplifier was replaced with a AD630 integrated circuit, which performed the same function as the bench top lock in. Output of the lock in was monitored with an ordinary multimeter.

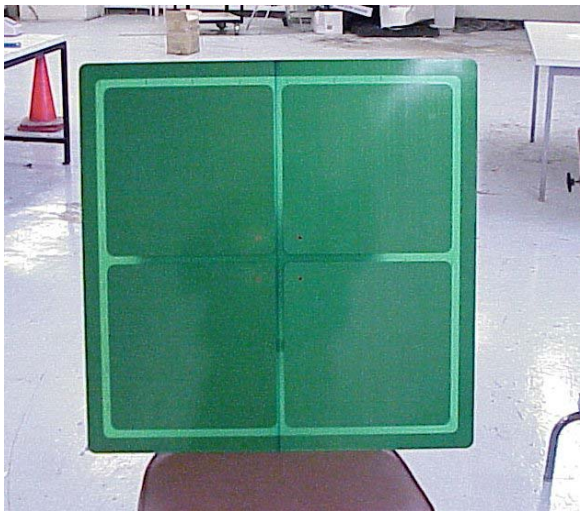

Figure 2. Experimental 4-Element Capacitive Tomography Array

In order to boost the amplitude of the drive signal applied to the sensor array a means of eliminating the common mode voltage had to be found. Several approaches were tried and discarded. An acceptable solution was found to be the construction of a transformer with a center tapped secondary winding. The center tap on the secondary allowed for a signal ground to be established close enough to the signal amplitude at the center of the bridge elements as to not overload the signal conditioning electronics. A block diagram of the sensor array drive and signal conditioning electronics is shown in figure 3. The signal drive consisted of a Wavetek signal generator followed by an Elinco power amplifier. Signal conditioning electronics consisted of a differential amplifier followed by synchronous demodulation after which a

filtering stage was applied before being applied to a standard digital multimeter. The array was capable of detecting a 4-inch plastic pipe buried at 4.5 feet. Maximal signal intensity was approximately 40 – 100 millvolt.

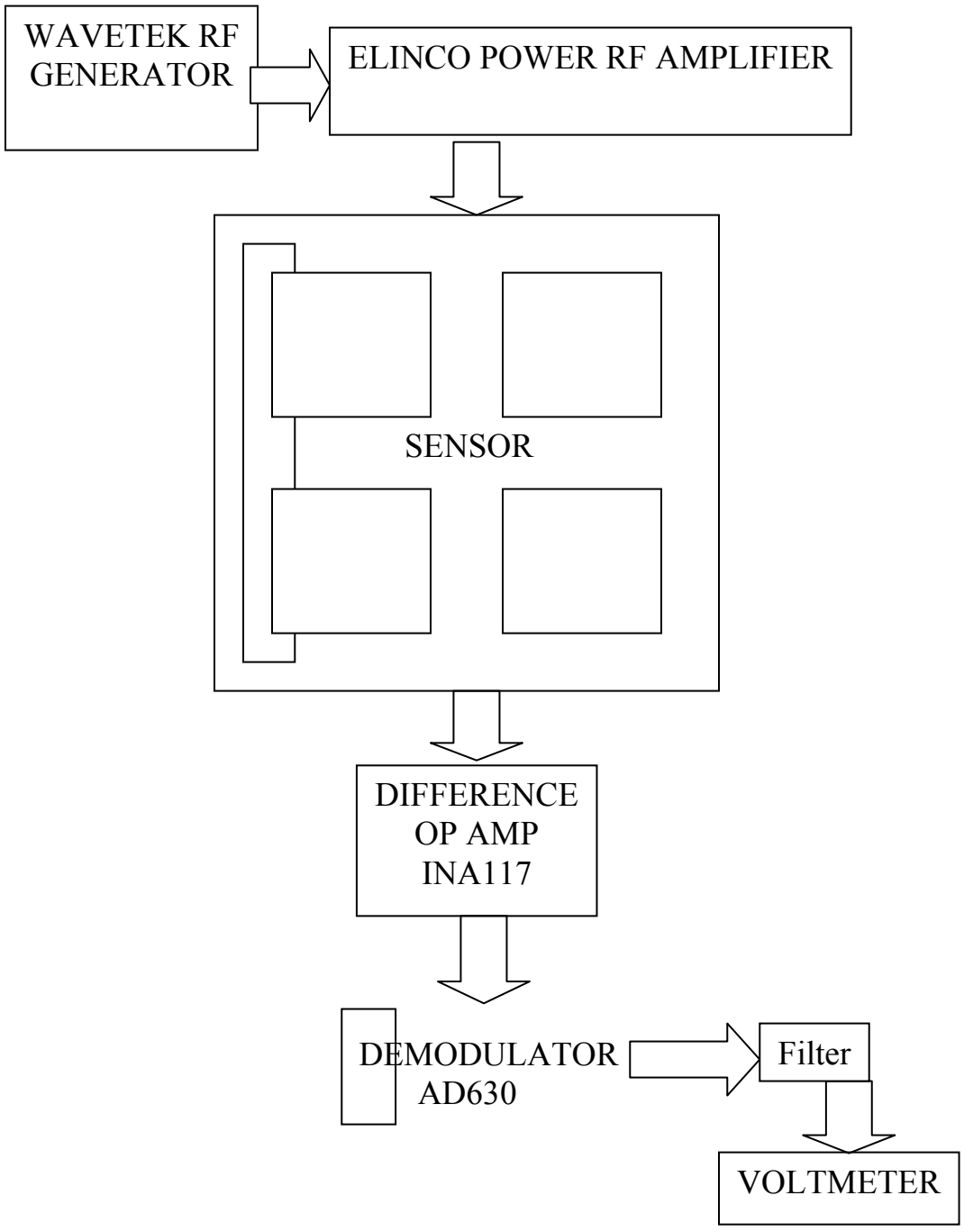

Figure 3. CT Block Diagram

In Figure 4 is shown the experimental set up for the testing of the 4-element sensor array. The testing was conducted in GTI's Soils and Pavement Laboratory. The array was tested over a test soil pit. The test pit is 20' x 20' x 8' and currently filled with a sand clay mix, which was chosen to be typical of the type of soil used for gas line back fill.

A wooden frame was constructed from ¾ in. x 3-in. clear white pine. Wood was used instead of metal because of the need to minimize potential interference with the electric fields. The frame's dimensions was 4' x 8'. The frame lays on the ground surface over the test pit. A 4" plastic pipe is buried 3 feet deep and runs perpendicular to the length of the test frame. The 24-in. square PCB capacitive sensor is mounted to two wooden cross beams. The sensor and wooden cross beams sits on the 4' x 8' wooden frame that allows the sensor to glide smoothly over the surface of the ground. A close up of the arrangement is shown in Figure 5.

Figure 4. 4-Element CT Array in GTI Soil Lab

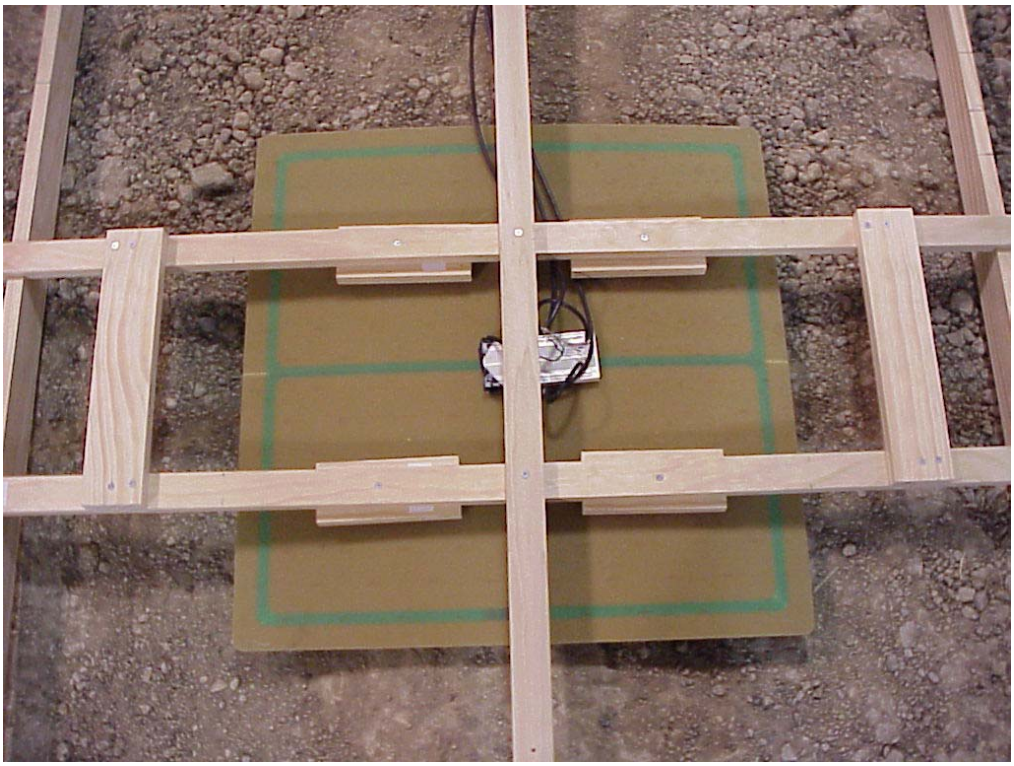

Figure 5. Close-up of Sensor on Sliding Frame

Initial results from the indoor soil pit testing were very encouraging. A very significant voltage maximum was detectable when the sensor was directly over the plastic pipe. Detailed voltage versus position data was taken, as shown in Figure 6. These measurements strongly indicate that the buried plastic pipe is readily detectable. Several sets of data were taken with various drive voltages and frequencies. Additionally several alternative methods of driving the sensor plates were looked at, all with good results. Spatial resolution of the detected signal was on the order of less than ½ an inch. There was at least an order of magnitude increase in the detected signal for the buried pipe as compared to the detected signal of a plastic pipe in air. This is due to the greatly reduced impedance of soil vs. air as the medium in which the plastic pipe resides.

Transitioning to Digital Instrumentation

Given the encouraging results obtained with analog instrumentation, the apparatus was transitioned to digital data acquisition. The purely analog approach is workable only with small numbers of sense elements. The need to go to higher element counts requires the use of digital technology.

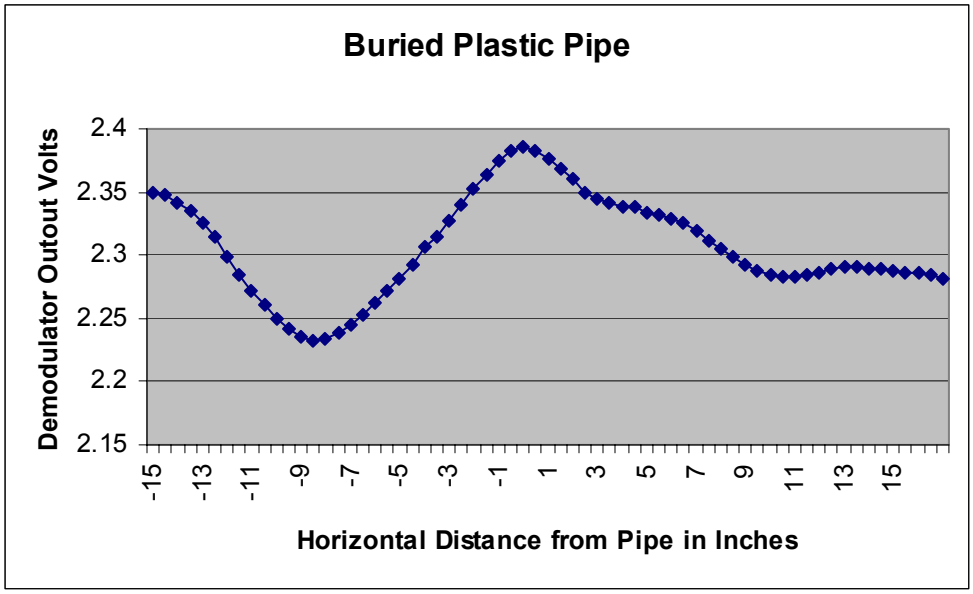

Figure 6. Signal Graph of 4-Element Sensor Moving Over Plastic Pipe

The National Instruments LabVIEW development environment was chosen for the data acquisition, signal processing, and graphical user interface. National Instruments data acquisition boards were examined for a product that would fulfill the need. A 6115 DACQ was chosen which could simultaneously digitize four channels of analog data at a maximum of 10 mega samples per second. With a drive frequency of 100khz to 400 kHz this would result in a range of 100 samples per cycle at 100 kHz and 40 samples per cycle at 400 kHz, well above the minimum Nyquist sampling rate of 2 samples per cycle. A Dell workstation was purchased with a 2.2 GHz CPU, a SCSI hard drive interface and a second dedicated hard drive for data storage. LabVIEW 6.1 Professional and MatLab were installed.

The project plan was to interface one sensor plate of the capacitive sensor to each of the four analog channels of the DAQ. A LabVIEW Virtual Instrument (VI) was constructed to allow the sensor signal data to be digitized and streamed to the hard drive in the PC. Going into the future it was anticipated that a 16-element sensor would be fabricated. A four to one

multiplexing would be implemented to map the 16 array plates to the 4 DAQ analog channels. Multiplexing of the sensor data was achieved through a discrete chip analog multiplexer.

Initial development of the VI for the NI 6115 DAQ went forward after the 6115 DACQ board arrived and was installed in the workstation. Evaluation of possible data acquisition and processing algorithms began. The board and software drivers were installed and initial tests were performed to verify operation. Various LabVIEW VI's were loaded and the DAQ was tested with these VI's with a 100 kHz signal input. Various scan rates and data refresh rates were tried to find the optimal settings for good signal representation. Data storage protocols were examined for there efficiency, speed, and readability. Storing the captured data to spreadsheet format allowed for the export of the data to third party applications such as Excel and MatLab. The stream to binary data storage protocol is fast and efficient, but currently only Lab View can read this data.

The ultimate goal of the LabVIEW development effort was to reproduce the results obtained from small element count arrays with more complex arrays. The analog signal processing used for small numbers of elements was replaced with digital signal processing for greater element counts to be feasible. LabVIEW provides a customizable user interface that lends itself into translating the signal data into a usable image.

16-Element Sensor Array

Following the good performance of the 4-element sensor array a 16-element array was designed and fabricated. The 16-element array was also fabricated on a 24” by 24” circuit board panel but with smaller elements. There was an important change between the 4 and 16 element array. The return signal path for the 4-element array was placed only around the outer perimeter of the array. The 16-element array uses a mesh type geometry wherein each of the 16 elements is surrounded by the return path. This change was made in order to create a uniform electric field line distribution around each of the sensor elements. This sensor is composed of sixteen 4.5 inch square sense elements embedded in a ¾ inch ground mesh. Each element is driven through a capacitor. Presently the drive capacitor is a variable capacitor of 1.4 - 5 pf.

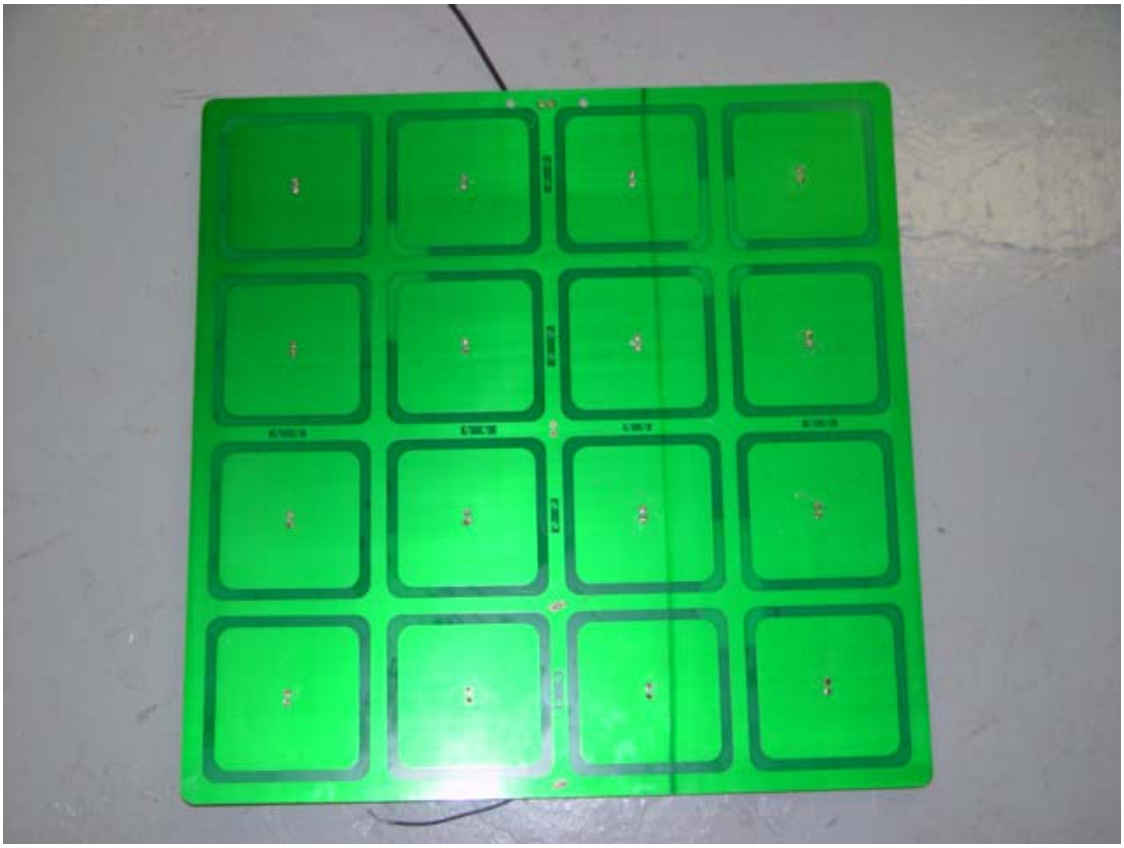

Figure 7. 16 Element Sensor Array

The signal drive design schematic is shown in figure 8. The drive chain is composed of an RF generator, followed by a power amplifier. The signal is fed into a center tapped secondary transformer. The RF is then fed to each sensor element by a discrete variable capacitor. It is important to note that the center tap of the transformer secondary establishes the signal ground. The return path (mesh) of the sensor is array is shown connected to the top of the transformer diagram.

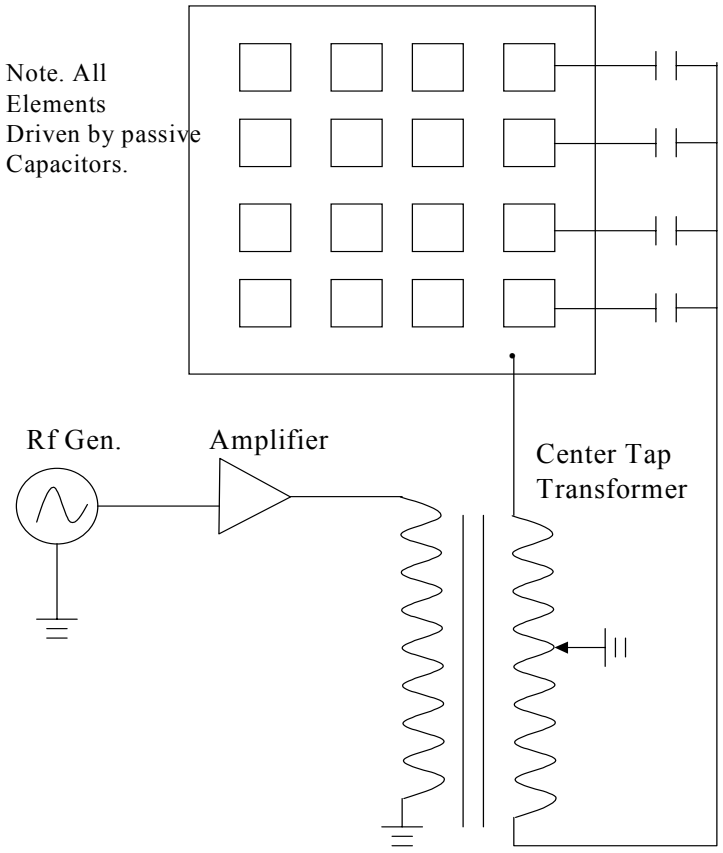

Figure 8. Drive Configuration for CT Sensor.

Figure 9 shows the complete system block diagram. Shown here is the 16-element sensor board the buffering and multiplexing circuit board, which is mounted to the sensor board, the data acquisition and processing board, which resides in the pc, and the LabView driver and GUI software. This arrangement allows any pair of sense elements to be routed to inputs on the DACQ card within the PC.

An electronic breadboard was constructed using two 16 to 1 multiplexers. The multiplexers allow any one of 16 sensor elements to be chosen with a 4-bit address bus. This address bus is driven from the digital output lines of the National Instruments data acquisition board. After debugging and optimal signal level was achieved the breadboard circuitry was transferred to a Vector circuit board so that it could easily be mounted to the sensor. Each element was connected through shielded coax to a 0.1-inch center standard header mounted on the Vector circuit board.

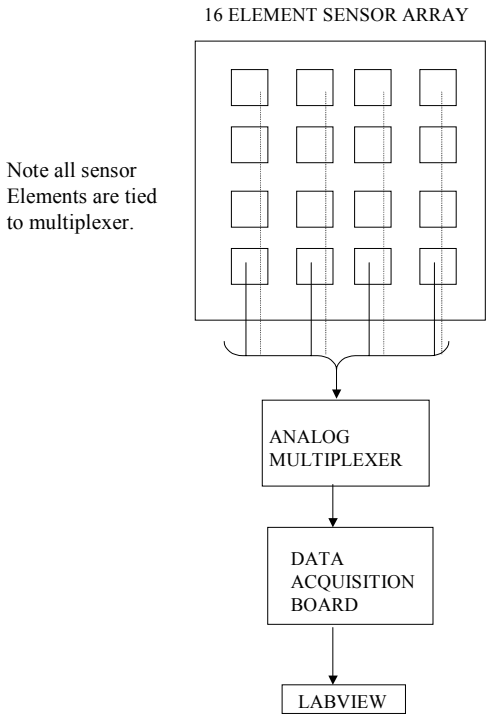

Figure 9. CT Sensor with Multiplexer

The block diagram of the LabVIEW software Virtual Instrument (VI) used to drive the signal conditioning hardware is shown in figure 10. This VI performs two main functions. The first function is to output addresses on an 8 bit addressing bus connected to the address pins on the analog multiplexer. The second function is to acquire the sensor signal from each of the sensor elements after a unique address has been sent to the multiplexer.

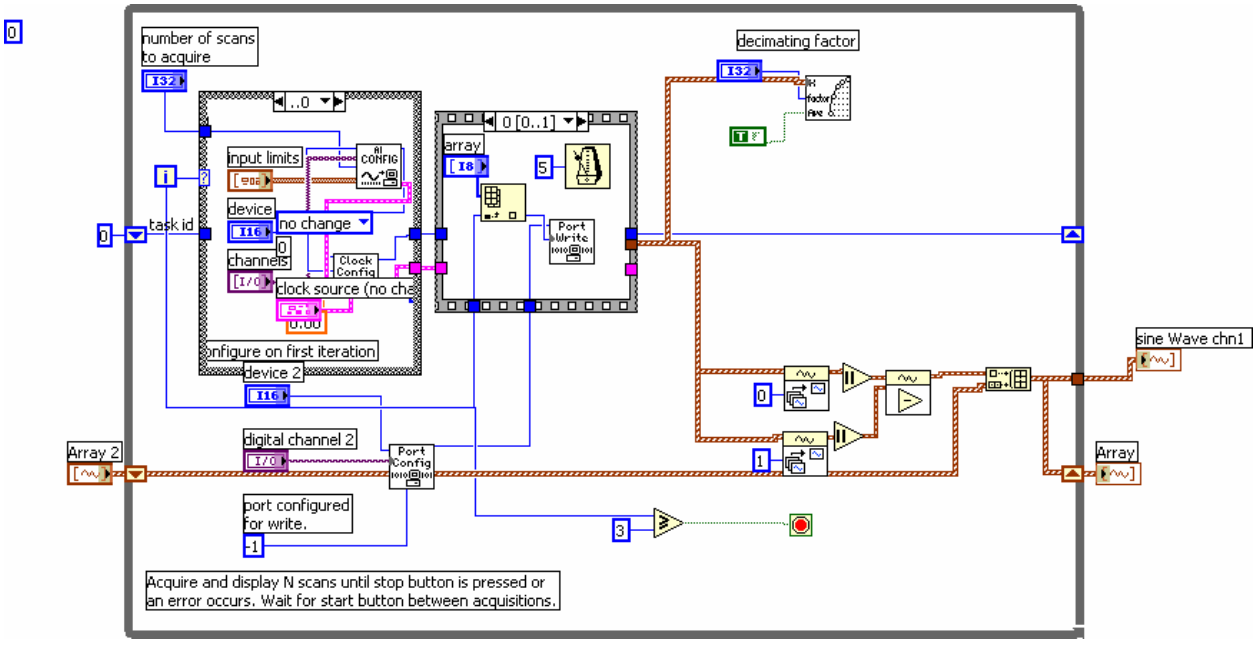

Figure 10. LabVIEW Data Acquisition VI

In figure 11 is shown a data collection session on GTI's outdoors buried pipe facility. In this picture the sensor array is locating a 6inch diameter plastic pipe buried at a depth of 4.5 feet. The sensor array in the foreground is tethered to a cart in the background, which contains the RF generator, RF amplifier, and PC with data acquisition card and LabView software.

In this particular instance, the array sensitivity was being calibrated. For this procedure the array was moved with respect to the buried pipe. Readings were taken at 1-inch intervals. Figure 12 shows a representative graph of data acquired in this manner.

Figure 11. Plastic Location on GTI Outdoor Facility

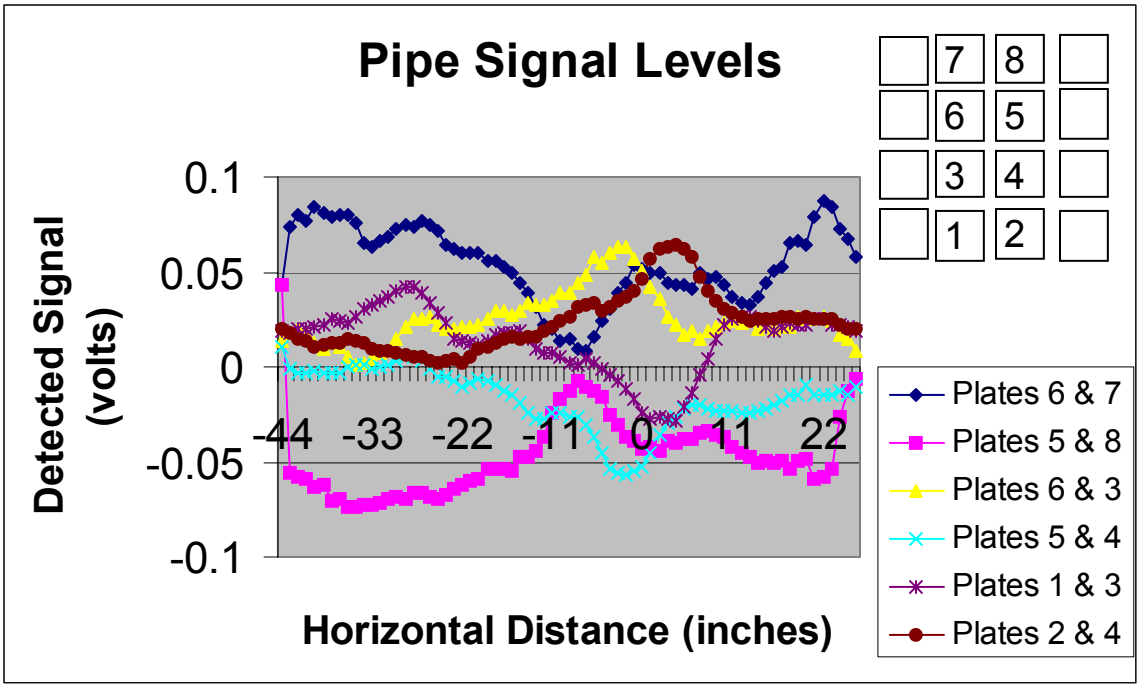

Figure 12. Data from Outdoor Facility Test

Buffer and Multiplexer Board

Following successful testing and development of the breadboard multiplexer and buffering circuit, it was transferred to a printed circuit board. The sensor elements must be sequentially scanned in order to build up an image of what is beneath the sensor. Several items of support electronics are required to accomplish this. Amplification is required to raise the sensor signals to detectible levels and to "buffer" the signals from outside interferences. A multiplexer is required to select the sensor elements singly or in pairs. Also, appropriate connectors and cabling must be provided to route signals to the appropriate points.

The multiplexer and buffer circuit board was designed at GTI and sent out for fabrication. Figure 13 shows the completed board with multiplexers and buffering amps installed. Testing of the board showed no defects or design errors and the board performed exactly as expected. This board implements the multiplexing, buffering, and amplification for 16 analog input channels. Figure 15 shows the basic system configuration that the board fits into. Each channel is connected to a sense element on the sensor plate. Using the multiplexer to scan these elements sequentially allows an image to be built up.

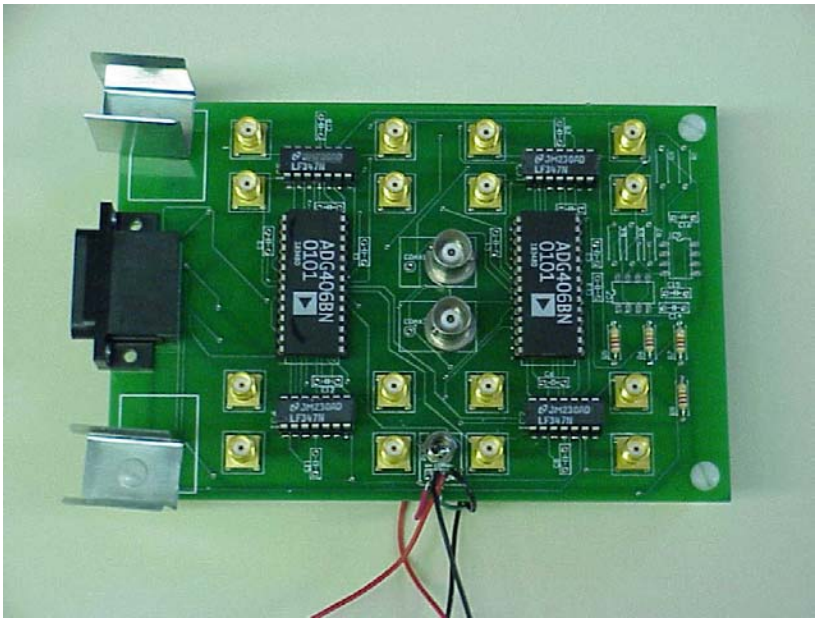

Fig. 13 CT Buffer and Multiplexer circuit board

An 8-bit address bus drives scanning of the 16 channels. This address bus is driven from a National Instruments 6115 DAQ board inside of a PC. The multiplexer board has two analog output channels, which are passed to the analog inputs of the 6115 DAQ board. The circuit board

had included several alternative component sets. These being the option to access one or two channels simultaneously, and the option to either pass each channel through a gain stage consisting of an LF412 or to pass pairs of channels through an AD621 differential instrumentation stage. Currently the LF412 with a gain of 10 is being utilized, though field trials have shown that this may make the array too sensitive. Good array response has resulted from driving the output coax lines to the DAQ straight from the multiplexers without the AD621 or the LF412 in the circuit.

The multiplexer board utilizes threaded SMA coaxial connectors to connect the sensor elements to the buffer stages. This connection method has significantly improved the physical robustness of the sensor signal pickup interface as well as improved the electrical signal integrity and noise immunity. A critical improvement was the addition of active shielding of the signals from the sensor elements to the input of the buffer amplifiers. Guard traces running parallel to the sensor input lines on the multiplexer/buffer circuit board were added in order to shield the sensitive input traces from electrical noise. This shielding is extended from the SMA connector to the sensor element connection by driving the coax shield by the output of the buffer as well. These traces and the shielding of the coax lines to the sensor elements were actively driven by the output of the buffering amplifiers. This in effect drives the shielding to the same potential as the sensor element.

RF Amplifier

Over the course of the project a consistent problem has been the need to drive the sensor array from a low frequency RF signal source with specific requirements.

1. A signal source with amplitude of at least 100 volts
2. A signal ground at ½ of the drive voltage
3. A flat amplitude over the range of 100kHz to 500kHz

The previous solution to this had been to use a custom designed transformer to interface an existing RF amplifier to the sensor. This RF amplifier, though large and heavy, was available and its performance was flat and dependable. When the need arose to scan a range of frequencies it became apparent that both the RF amplifier being used as well as the transformer exhibited a frequency response that was not constant. Up to this point the range of frequencies that could be swept was limited, because of the non-flat response of the RF amplifier used.

In order to solve this problem a solid-state high voltage RF amplifier was constructed using two APEX OP85 high voltage operational amplifiers. With these operational amplifiers configured in a bridge drive arrangement all of the above mentioned requirements were met. In addition the physical size of the amplifier was reduced by a factor of 10 and the power requirements were greatly reduced and simplified. This amplifier can also be driven by a battery power source, which would allow this to used in a battery powered sub-surface imaging system.

Utilizing the multiplexer and buffering board shown in figure 13 and the RF amplifier shown in figure 14 resulted in a significant improvement in signal resolution and amplitude. These improvements can be seen graphically in figure 15.

Further improvements were made to the RF bridge amplifier. The bandwidth over which a flat response could be obtained was expanded from 100 kHz - 200 kHz, to 100 kHz –400 kHz. This was accomplished by an adjustment of the value of the bias resistors used in the unity gain stage of the bridge amplifier. This greatly expanded the depth sensing capabilities of the CT sensor.

Fig. 14 Apex Solid-State RF Amplifier

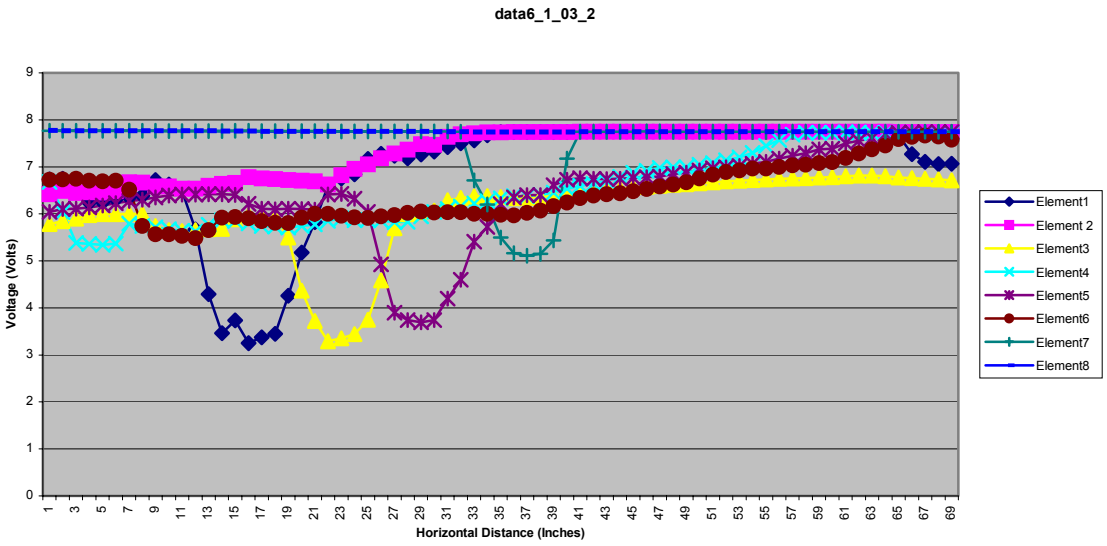

Fig 15. Signals from 6” plastic pipe at depth of 50”

LabVIEW Code for CT Scanning and Imaging

In figure 16 is shown the block diagram for the CT scanner and imaging software. The basic functions indicated is the acquisition loop, which drives the analog multiplexers and concurrently acquires and processes the 16 sensor element signals. The GPIB driver handles the signal generator frequency hopping functions. The image driver loop is responsible for displaying the sensor signal data in a visual color-coded topographic mapping.

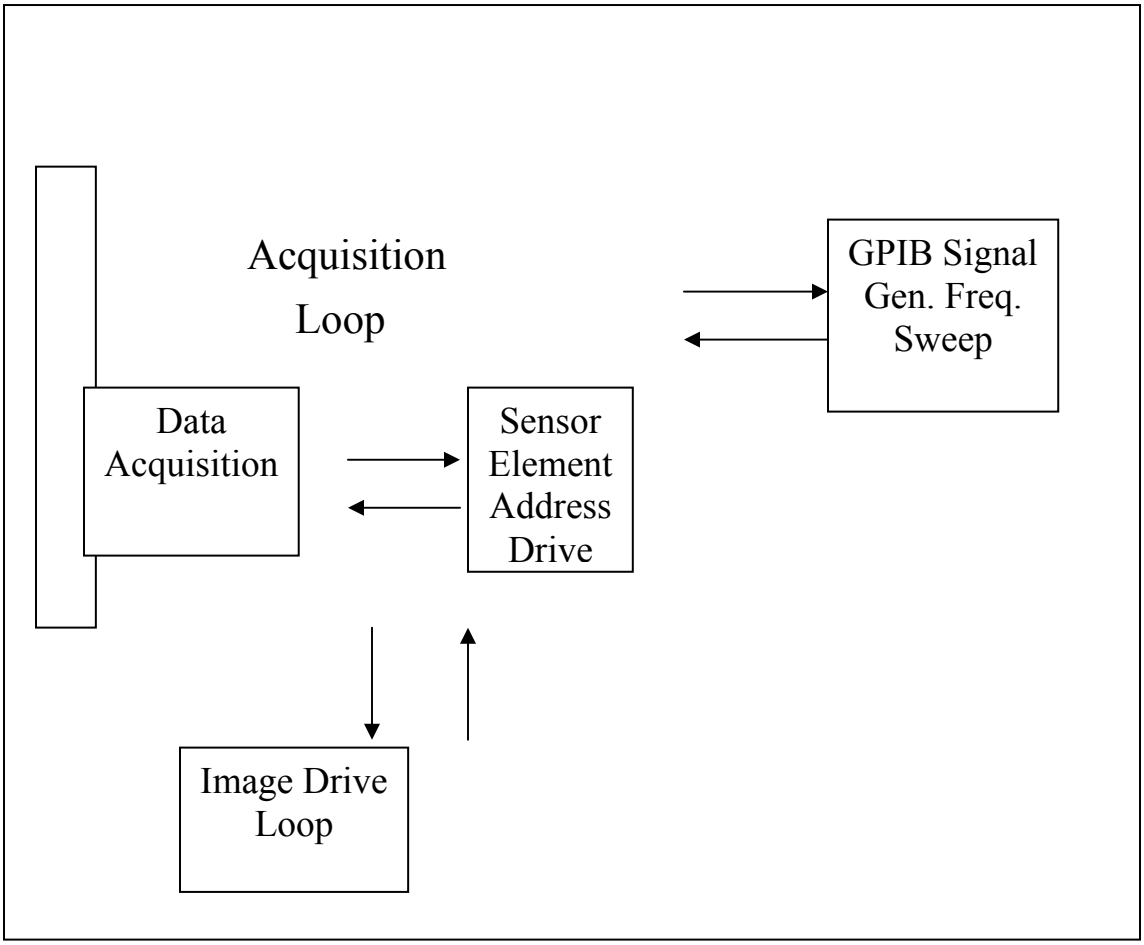

Fig. 16. CT Software Block Diagram

Figure 17 shows the LabVIEW code diagram that implements the functions shown in the block diagram. The outermost boundary is the main system loop, which insures that each of the smaller loops inside of it is continually executed in order. The large loop on the left corresponds to the data acquisition and addressing functionality. The loop on the right drives the imaging display. The small loop at the top handles the GPIB interface to the signal generator. Each of these loops will be described in some detail.

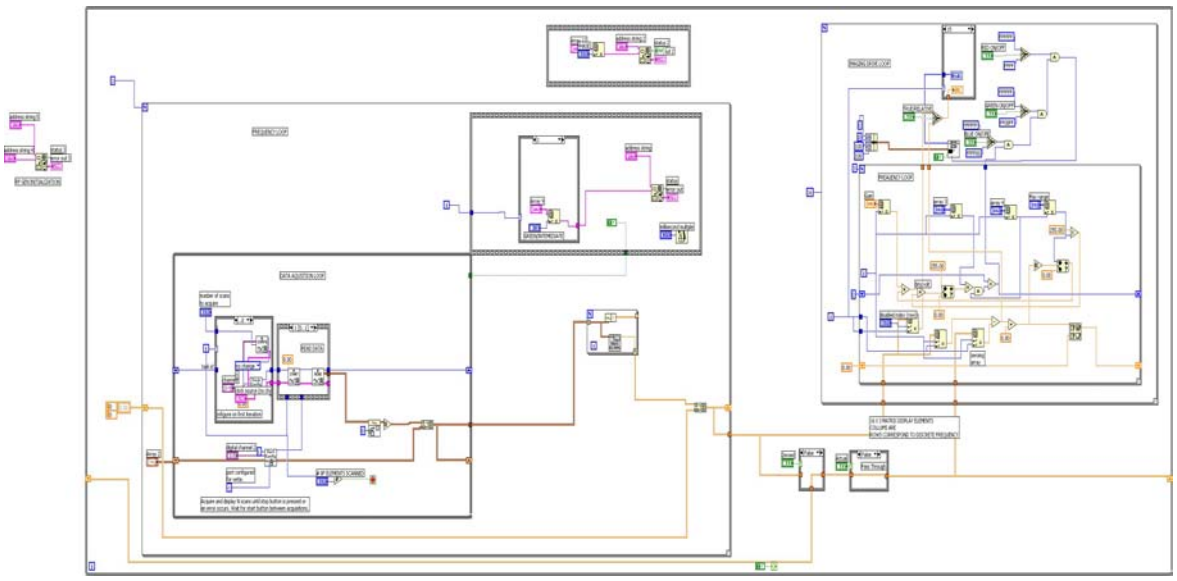

Fig 17. Acquisition and Driver VI Overview

In figure 18 is shown the acquisition and address driver code for the CT sensor multiplexer and buffering board. The case structure on the left (inside the outer while-loop) configures the data acquisition card channels, clock source, and trigger source. To the right of this case structure is a sequence structure which containing two sequence elements. The first element is shown in Figure 18 and acquires 500 samples from a sensor element.

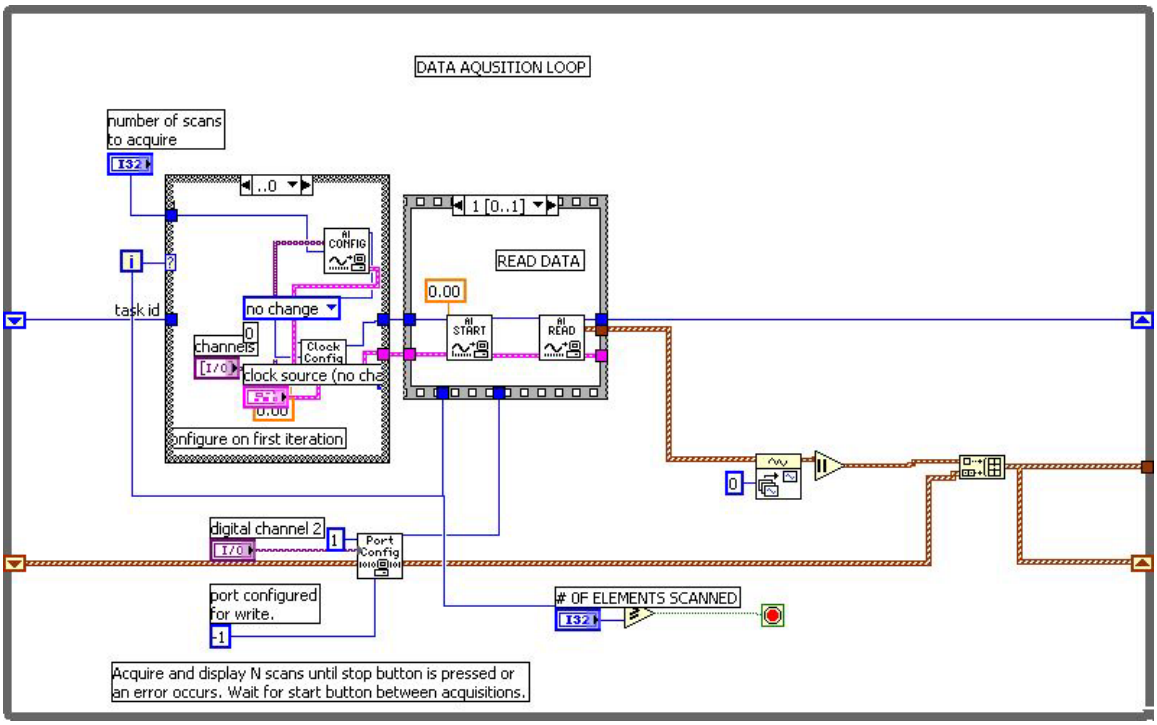

Fig. 18. Acquisition Loop Showing Data Read Element

The next sequence element shown in Figure 19 drives an address out to the analog multiplexer that determines the particular sensor element that is being addressed. The other elements in the while loop build an array of sensor values that results from the multiple iterations of the loop.

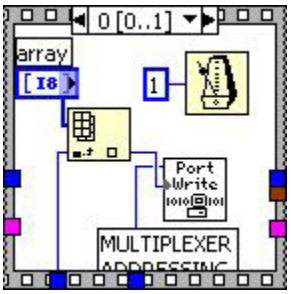

Fig. 19. Sequence Element for Multiplexer Addressing

In figure 20 is shown the sequence structure containing the code to adjust the signal generator frequency via GPIB. Three discrete frequencies are used, each corresponding to one of the case statements as shown. Inside each case statement is an array that contains a vector of text messages to be sent over the GPIB channel to the signal generator. The array of text messages allows the operator to change the frequency by changing the index of the array from a control on the front panel.

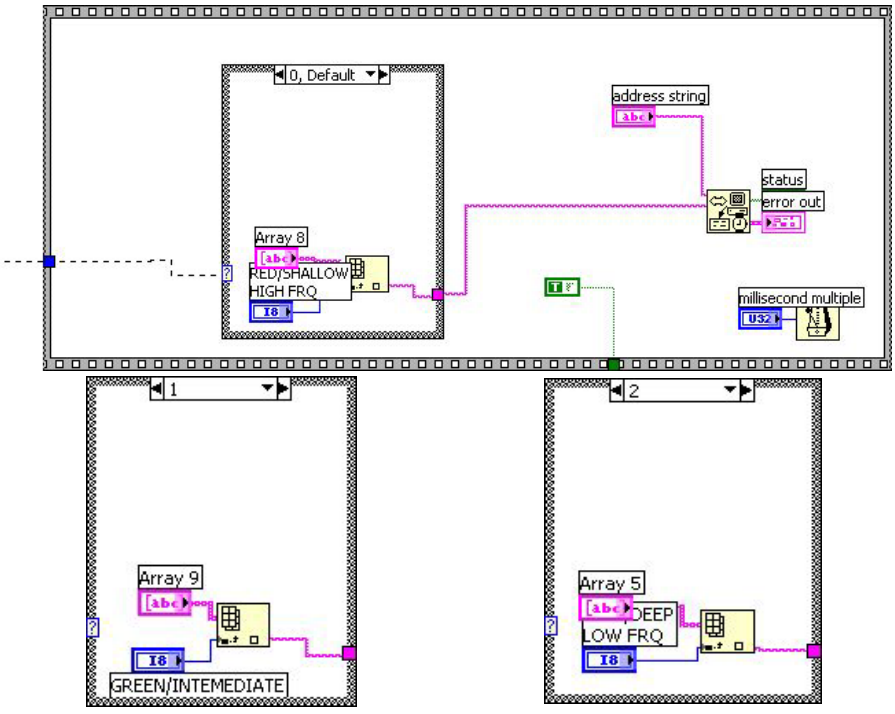

Fig. 20. Code Sequence for Frequency Control

The LabVIEW code shown in figure 21 is primarily responsible for driving the imaging GUI for the CT scanner. It consists of two while-loops. The outer while loops executes 16 times: once for each of the 16 sensor elements. The inner loop executes three times: once for each of the frequencies to be scanned for depth determination. The case structure contains 16 instances: one for each of the display elements and the numerical value display for the signal value acquired. The three AND function to the right of the case structure perform the merging of the three distinct colors corresponding to depth data. The one resultant color index is mapped to the proper display element.

This code also contains provisions for auto zeroing where a scan is taken for the ground at all three frequencies and subsequently all further scans have these values subtracted out. An auto scaling function is implemented here so as to optimize the sensitivity. This functions by setting the maximum value for a given frequency and then scales the color mapping functions for this value.

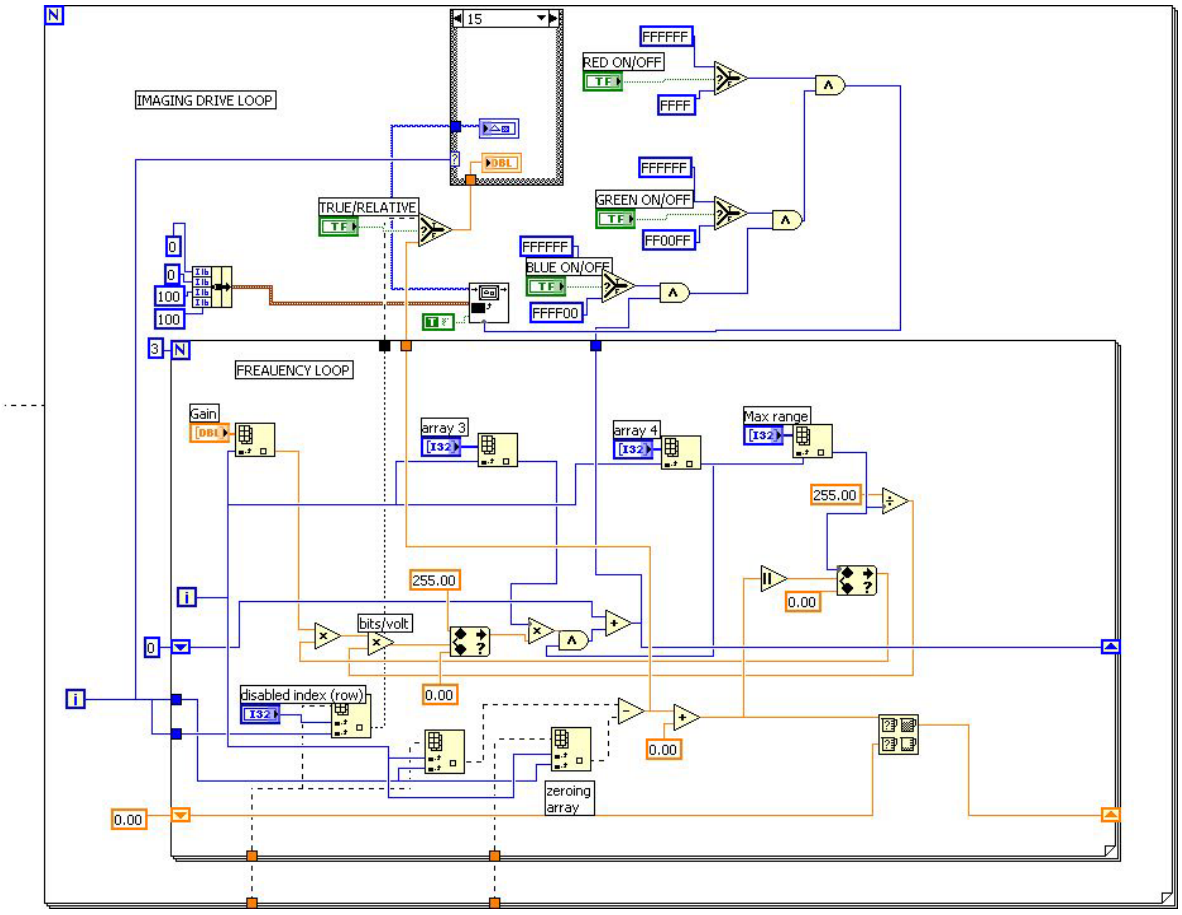

Fig. 21. CT Code for Imaging Functions

Two Dimensional Imaging

The following screens show representative imaging of the pipe. In this mode, the array is left stationary on the ground. The soil is scanned and the impedance differences between adjacent sense elements are mapped into colors. In Figure 22, the array has been moved with respect to the pipe. Elements 3,4,11, and 12 are showing the location of the pipe directly below these elements. In figure 23 elements 11, 5, and 8 are excited indicating a pipe running from the lower left to the upper right under the excited elements.

These "large pixel" images, while coarse, are easy for the operator to interpret. They are recognizable the outline or silhouette of an object beneath the sensor array. This is in contrast to a standard GPR display shown in Figure 24. This diagram shows a single "slice" through an area with buried features. The parabolas indicate reflections off buried objects and require significant operator expertise to interpret correctly.

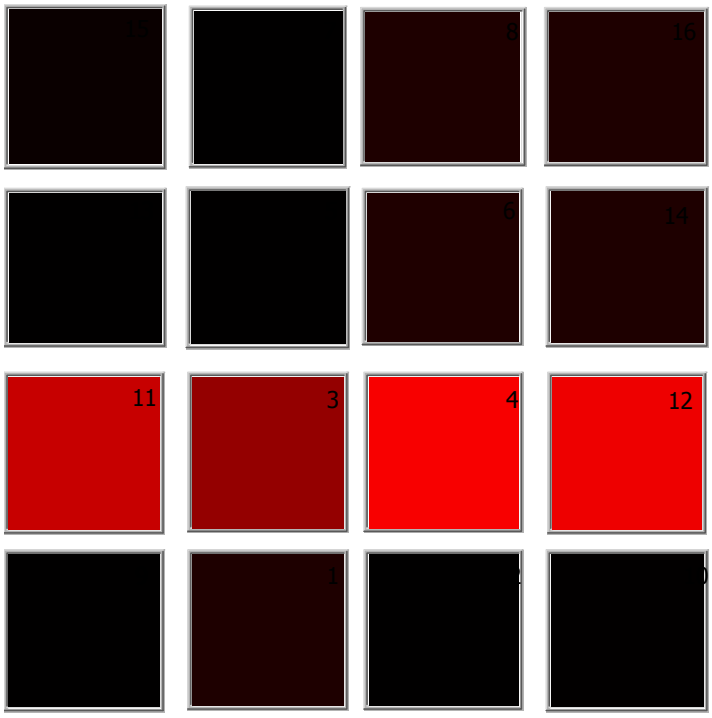

Fig. 22. Pipe Perpendicular to Array

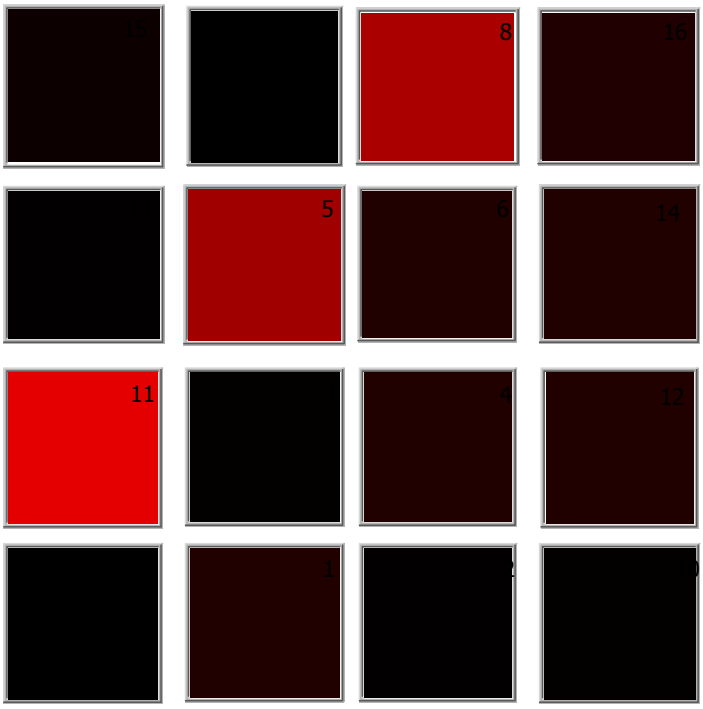

Fig. 23. Pipe Diagonal to array

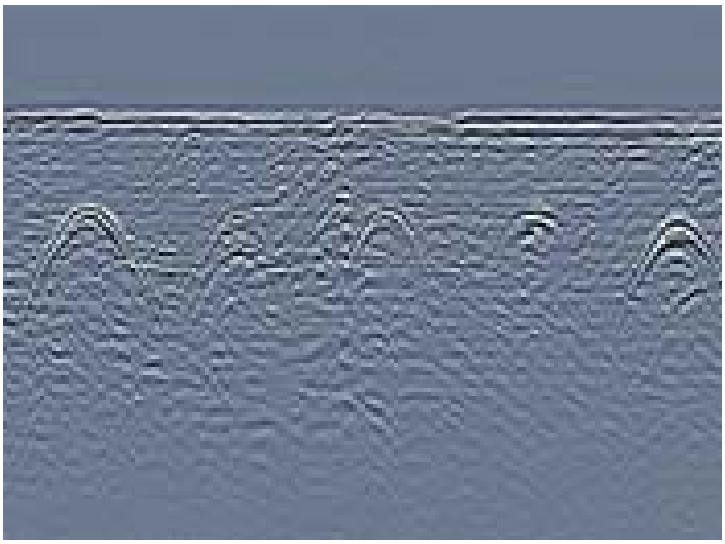

Fig. 24 Standard GPR Data Display

64-Element CT Sensor Board

Experience gained from the 16-element array has allowed the completion of the 64-element sensor array. This increase in the number of sense elements will correspondingly increase the resolution of the image generated. This array is composed of 64, 2"x 2" sensor elements embedded in a grounded mesh. The backside of the sensor array has integral RF drive signal distribution.

The new 64-element sensor board, shown in Figures 26 and 27, has incorporated several design enhancements, such as the implementation of the buffering and multiplexing functionality directly on the topside of the sensor board. The 64-element board uses surface mount quad op amps and multiplexers that mount directly to the top surface of the sensor to reduce the size and complexity of the support electronics.

The 64-element sensor divides the array into functional groups of 16 elements with their own local multiplexer and buffering amplifiers. A quad LF412 amplifier is located at the center of every 4 sense-element group. At the center of every 16 sense-element group there is located a 16 to 1 multiplexer to gather the output of the 4 quad amps into one channel. A close-up of such a group is shown in figure 27. The 64-element sensor board uses 16 quad op amps and 4 sixteen-channel multiplexers.

In addition to simplifying the wiring harness, the use of surface mount components should help normalize the sensitivity of the array elements. Some of the variation now seen can be attributed to the cabling between the sense elements and the first stage of amplification. Long cable runs produce a parasitic capacitance in parallel with the sense element. The additional capacitance decreases the sensitivity in a less than predictable fashion. Additionally it is anticipated that this normalized sensitivity will allow the sensor design to replace the variable tuning capacitors with a fixed capacitance drive configuration.

The 64-element sensor array is composed of four layers. The first layer or bottom of the board is composed of the 64 sense elements and the mesh that surrounds the sense elements. This layer is shown in figure 26. Each of these elements is approximately 2" x 2". The next layer up from the bottom sense layer is the RF drive layer, this layer routes the drive signal to the 64 elements via the variable tuning capacitors. The next layer up from the drive layer is the shielding layer tied to the bridge ground. It is expected that a greater uniformity of electric field distribution will result from this arrangement. This uniformity should translate into a flatter response from one element to the next for a given signal. This also decreases the number of elements that lie on the edge of the array, where sensitivity is lower.

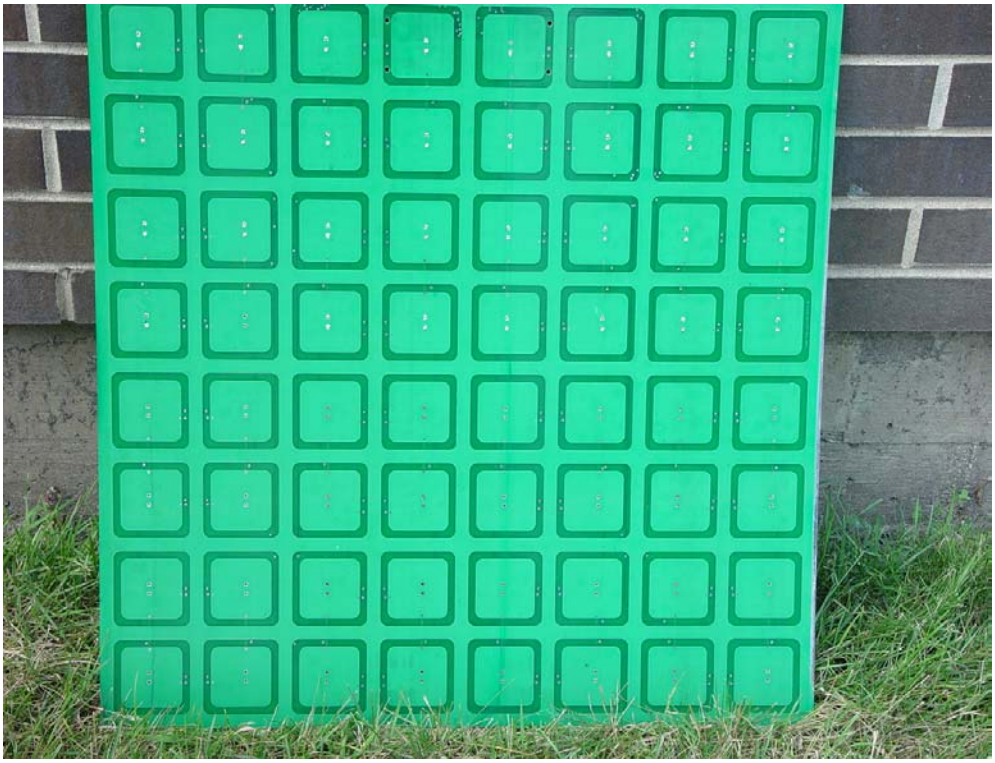

Fig. 25. Sensor Side of 64-Element Array

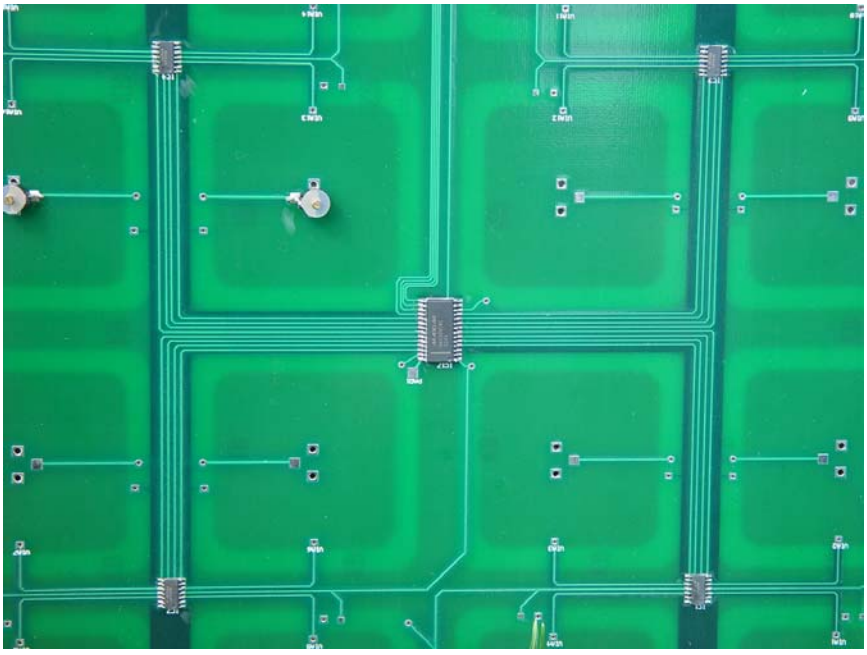

Fig. 26. Integral Surface Mount Support Electronics

Code was developed for the 64-element sensor board. This code is very similar to previous code except it now is scanning 64 elements instead of 16. There was concern before the 64-element board went out for fabrication that the speed of the PC would not scale up to accommodate the additional elements. The code was implemented and is now acquiring 64 elements. The display is shown in figure 28. The display update speed did slow down by approximately 50% but still updates the entire screen in less than a second. This does not significantly impair the usability of the GUI.

Initial testing of the 64-element board was completed. All of the circuitry functioned properly. Connectors were installed to enable the board to be interfaced to the data acquisition board and the addressing drivers. Initial testing indicated that power was being distributed properly the surface mount components. Single element sensitivity measurements were performed with signal fluctuations of 50-100 millivolts. Further development was halted given time and budgetary constraints. A tactical decision was made to use the 16-element sensor for an upcoming demonstration as it was better developed.

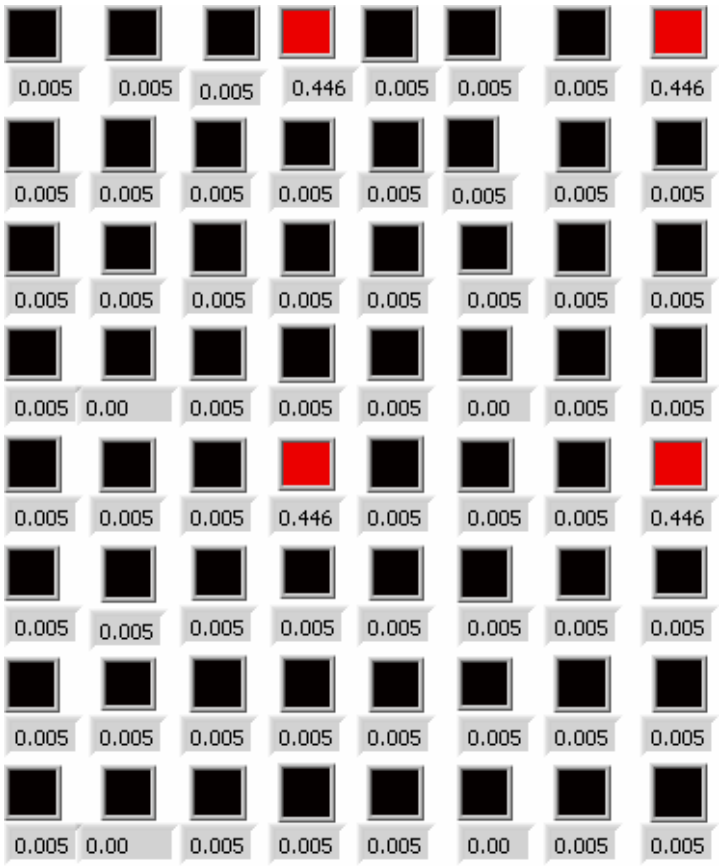

Fig. 27. Screen Shot of 64-Element Display

Public Demonstration of Capacitive Tomography

In order to facilitate the practical imaging of a plastic pipe in the field, the 16-element sensor array was mounted to a wheeled cart. The cart is shown in the following figures. This cart is constructed of wood and has an aluminum handle that allows the user to easily lift the array off the surface move it to the area of interest and set it down. The array rests on a 1/8-inch thick sheet of anti-static polycarbonate mounted to the bottom of the cart. The cart was constructed so that on flat ground there would be a 1/8 of an inch air-gap. Obviously in most field test situations the ground is not perfectly flat and it is expected that there will be some variation in the air gap. An additional set of wheels was later added to the front of the cart, enabling a more uniform air gap to be maintained. This also reduced the impedance variations that were introduced by ground surface variations.

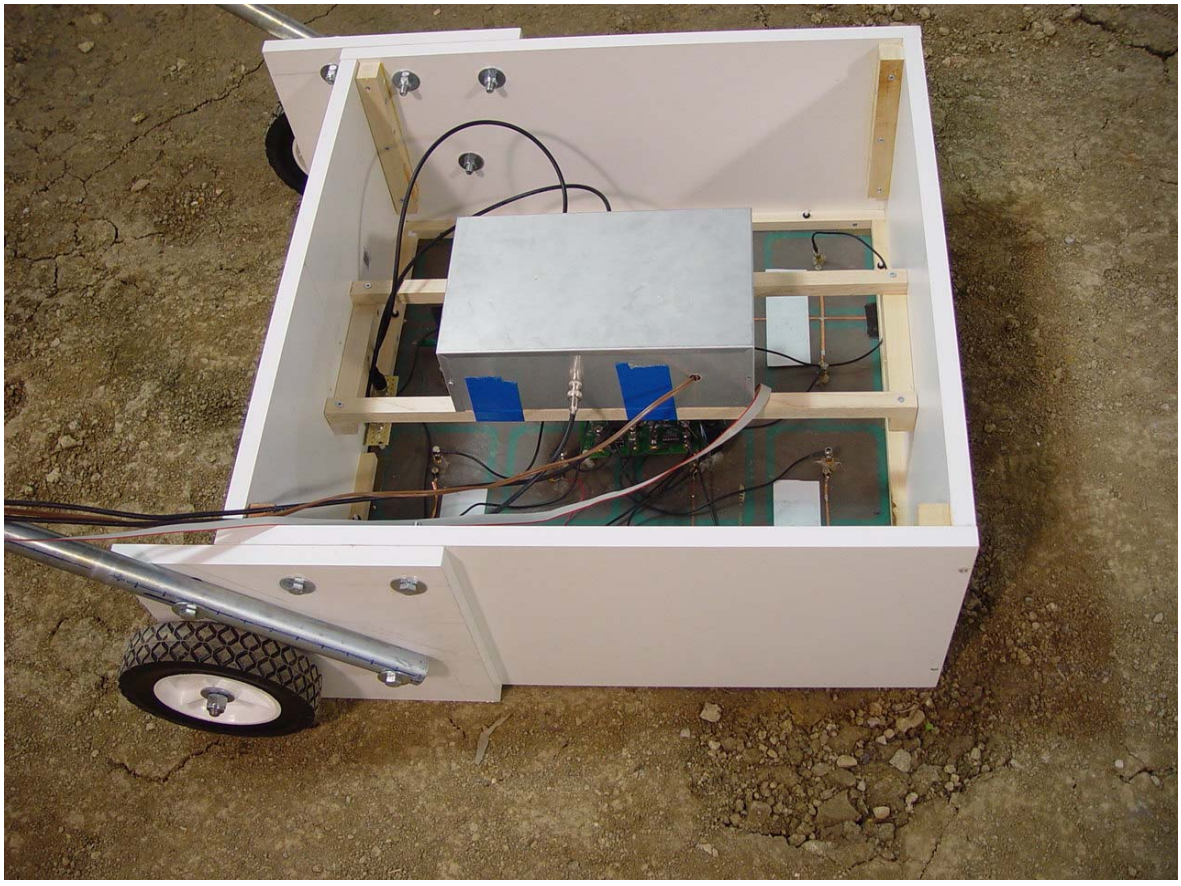

Fig. 28. 16-Element CT Sensor Mounted on Cart

The CT sensor array and cart was demonstrated at the "Underground Focus Live" conference at Manteno Illinois. Here the CT sensor compared its capabilities to that of ground penetrating radar (GPR). A number of buried plastic pipes were imaged with the CT sensor and two different GPR based devices. One GPR device had difficulty detecting a sample pipe that had been buried specifically for the UFL conference.

One aspect of the CT sensor was commented on by many of the UFL attendees: the simplicity of the display. A comparison of Figures 24 and 25 shows the contrast in the outputs of the two devices. The GPR display requires considerable expertise to interpret correctly. The CT display presents a coarse image with color-coding show depths.

Fig. 29. Bottom side of CT sensor array mounted to cart.

Depth Imagining Capability

A depth sensing and imaging capability was added in the final quarter of the project. The ability to scan at multiple frequencies was added early in the CT project, but imaging using these capabilities had not been developed. The principle is that different frequencies of excitation signal will propagate to different depths in the soil. Specifically, higher frequencies will attenuate more rapidly, giving less soil penetration.

The depth software that was developed scans three discrete frequencies. The CT response to each particular frequency was then mapped to a specific color. In this case the low frequency was mapped to red, the middle frequency was mapped to green and the high frequency was mapped to blue. The relative amplitude response of the CT sensor elements was mapped to the intensity of the color for a given frequency. The three colors were then added together and displayed to give topographical display. The VI included the capability to individually adjust the specific frequency values. Additional capabilities included phase and amplitude adjustment. Weighting adjustments were also added to account for variations in soil types.

An alternative 3d software imaging technique was also developed that utilized voltage thresholds to determine when a color contribution associated with a particular frequency would be made to the cumulative color displayed on the individual display elements. Code was written to determine when a detected signal for a particular frequency would fall above a user defined voltage threshold.

A sub-array processing algorithm was developed to divide the sensor into 16 sub arrays. Each sub array element's signal intensity would then be averaged together. There would then be 16 signal intensities. From these 16, the maximum amplitude was selected. The sub array elements corresponding to this signal would then be highlighted on the screen. This processing method offers some advantages in that a layer of abstraction or processing is inserted between the display elements and the sensor element signal intensities. This had the effect of filtering out or flattening the random signal variations that can occur from one sensor element to the next.

A DC bias removal algorithm was implemented in order to remove any residual DC bias on the sensor plates. It was accomplished by multiplying samples taken on the negative half of the sine wave to be multiplied by "-1", effectively rectifying the signal of interest. This was done in order to prevent dc bias from interfering with the depth resolution software.

Conclusions

- Capacitive Tomography provides a viable alternative to Ground Penetrating Radar for sub-surface imaging.
- CT has sufficient sensitivity to detect PE pipe in wet soils at depths greater than 4 feet.
- The technique uses a combination of phase detection and signal averaging to achieve the required sensitivity.
- The CT data display is easy for the operator to interpret. It does not require a great deal of operator training or post-processing.
- A 16-element array was demonstrated at the Underground Focus Live trade show where it was compared side by side with GPR.
- Several manufacturers at UFL expressed interest in the CT technology.
- The signal to noise ratio is sufficient that a 64-element array was designed and fabricated. Preliminary tests show very good sensitivity even with smaller individual elements.
- There is further development work needed on the 64-element sensor array. GTI will be seeking additional funds to bring CT to commercialization.

REFERENCES

In a patent entitled " Driven Shielding Capacitive Proximity Sensor", patent number 5,166,679, dated November 24, 1992, inventors John M. Vranish and Robert L. McConnell have presented an invention for a capacitive proximity sensor that will detect the intrusion of a foreign object into the working space of an electrically grounded robotic arm. The capacitive proximity-sensing element is backed by a reflector that is driven by an electrical signal of the same amplitude and phase as that signal which is detected by the sensor. It is claimed that by driving the reflector plate with the same signal that is on the sense element significant increases in the sensor's range and sensitivity are accomplished.

In a patent entitled "Steering Capaciflector Sensor", patent number 5,363,051, dated November 8, 1994, inventors Del T. Jenstrom and Robert L. McConnell, present an invention that will allow for the steering of the electric field lines produced by a capacitive type proximity sensor. The inventors assert the claim that by steering or focusing the electric field will allow an increased ability to discriminate and determine the range of an object in the area of observation over that of previous capacitive sensors. Differential voltages applied to shielding plates spatially arranged around the sensor plate accomplish steering of the electric field lines.

In a patent entitled "Buried Pipe Locator Utilizing A Change In Ground Capacitance", patent number 5,617,031 dated April 1, 1997 inventor John E. B. Tuttle has invented a portable buried pipe detection device that utilizes changes in the electrical properties of the soils surrounding underground pipes. The detection method consists of the injection of a low frequency sinusoidal wave into the ground via an array of injector/sensor plates. Subsequent modification of the injected signal by variations in ground impedance brought about by the existence of buried piping structures will result. The modified signals will be detected by the spatially separated sensor elements located on the device. The injector/sensor elements are constructed in such a manner as to comprise a capacitive bridge circuit when viewed in conjunction with the ground. As the detection array is moved along the ground any occurrence of underground piping structures will imbalance the capacitive bridge and give rise to a detectable electrical signal.

LIST OF ACRONYMS AND ABBREVIATIONS

CT - Capacitive Tomography

COR – Contracting Officer's Technical Representative

DOE - Department of Energy

FERC – Federal Energy Regulatory Commission

GPR – Ground Penetrating Radar

GRI – Gas Research Institute

GTI - Gas Technology Institute

IGT – Institute of Gas Technology

IRNG –Infrastructure Reliability of Natural Gas

PCB – Printed Circuit Board

IF – Intermediate Frequency

MDPE – Medium Density Polyethylene

VI – Virtual Instrument

NI – National Instruments

DACQ – Data Acquisition

GUI - Graphical User Interface

SNR – Signal to Noise Ratio

Appendix A. MatLab Code for Determining the Phase Sensitivity

```
%This function calculates various impedence parameters for two resistors
%and capacitors in series. More importantly it calculates the variation in
%voltage across the second impedance(Z2)due to a small variation in the
%capacitance of Z2. This is given by the input variable sm_del, which takes
%on values 0 < sm_del < 1. The basic equation is V2= [A][B] and
%V2_del=[A_del][B_del], A is the impedance due to the pure magnitude of the
%parameters, A_del is the same except calculated with C2 having changed a
%small amount. B is the voltage variation due to the phase factor and
%likewise B_del is that due to the addition of the variation in C2. At the
%end a subtraction is done to compare the voltage variation due to the
%change in magnitude and the change in phase. Assuming the code is correct
%where the reactance is greater than the resistance the phase factor
%predominates the reverse is true where the resistance is greater than the
%reactance. The drive voltage has been assumed to be 1 volt. Multiplying the
%Z_Mag_Change or Z_Phs_Change by the actual drive voltage gives the true
%ouput variation. The effect of the phase factor can not be seen if one is
%averaging over many cycles, if for instance one is taking one sample per
%cycle the phase effect is observable.

function Z_PH=Z_ph(C1,C2,R1,R2,w,sm_del)
%sm_del=0->1
X1=1./(w*C1)
X2=1./(w*C2)
X2_del=1./(w*(1+sm_del)*C2);
X2_dif=X2_del-X2;

XT=X1+X2;
XT_del=X1+X2_del;
RT=R1+R2;

Z1=R1+-i*X1;
Z2=R2+ -i*X2;

Z1_MAG=(R1.^2 + X1.^2).^0.5;
Z2_MAG=(R2.^2 + X2.^2).^0.5;
Z2_MAG_del=(R2.^2 + (X2_del).^2).^0.5;

Zt_MAG= ((R1+R2).^2 + (X1+X2).^2).^0.5;
Zt_MAG_del=((R1+R2).^2 + ((X1+(X2_del)).^2)).^0.5;
%Zt_MAG_differential=(Zt_MAG - Zt_MAG_del);

Zt_Phs = atan(XT./RT);
Zt_Phs_del = atan(XT_del./RT);
Z2_Phs = atan(X2./R2);
```

```
Z2_Phs_del = atan(X2_del./R2);

V2_Phs_sens = (Z2_Phs - Zt_Phs);
V2_Phs_sens_del=(Z2_Phs_del - Zt_Phs_del );

A=(Z2_MAG./Zt_MAG);
A_del=(Z2_MAG_del./Zt_MAG_del);
Z_Mag_Change =A -A_del

B=sin(V2_Phs_sens);
B_del=sin(V2_Phs_sens_del);
Z_Phs_Change = B-B_del
%V_sensor=(A)*(B)
%A=Z2_del./(Zt_MAG_del)
%B=ph_Tot


Z_PH=Zt_MAG;

function Z_deriv= z_der(z1,z2);
Z_deriv=(z1*z2+z2.^2)./(z1+z2).^3;
```

MatLab Code for Calculating the Derivative and Creating the above Plot.

APPENDIX B

The following is a derivation the output voltage and sensitivity for two resistors and two capacitors in series. The labeling conventions use the subscript words "Drive" and "S" to denote the drive capacitor, drive resistor, sensor capacitor, sensor resistor elements.

1.) $V_{Sensor} = I_{sensor} Z_{Sensor}$

2.) $Z_{Sensor} = R_s + iX_S$;

3.) $X_S = -i \dfrac{1}{2\pi f C_{Sensor}}$

4.) $Z_{Sensor} = |Z_S| e^{i\phi_S}$

5.) $|Z_S| = \sqrt{R_S^{\,2} + X_S^{\,2}}$

6.) $\phi_S = \tan^{-1} \dfrac{X_S}{R_S}$

7.) $I_{Sensor} = \dfrac{V_{Drive}}{Z_{Total}}$

8.) $Z_{Total} = R_{Drive} + R_S + i(X_{Drive} + X_S)$

9.) $Z_{Total} = |Z_T| e^{i\phi_T}$

10.) $|Z_T| = \sqrt{(R_S + R_{Drive})^2 + (X_S + X_{Drive})^2}$

11.) $$\phi_T = \tan^{-1}\frac{(X_S + X_{Drive})}{(R_S + R_{Drive})}$$

12.) $$V_{Sensor} = \frac{V_{Drive}}{Z_{Total}} Z_{Sensor}$$

13.) $$V_{Sensor} = \frac{V_{Drive}}{|Z_T| e^{i\phi_{Tt}}} |Z_S| e^{i\phi_S}$$

14.) $$V_{Sensor} = \frac{V_{Drive}}{|Z_T|} |Z_S| e^{i\phi_R}$$

15.) $$\phi_R = \phi_S - \phi_T$$

Assume V_{Drive}=0, and the magnitude factor is $\frac{|Z_S|}{|Z_T|}$. From previous derivation eq. Shows that

16.) $$\frac{|Z_S|}{|Z_T|} = \frac{\sqrt{R_S{}^2 + X_S{}^2}}{\sqrt{(R_S + R_{Drive})^2 + (X_S + X_{Drive})^2}}$$

17.) $$\frac{d(\frac{|Z_S|}{|Z_T|})}{dx}$$

The derivative of eq. 17 is given by

18.) $$\frac{d(f_1(x)/f_2(x))}{dx} = \frac{f_2(x)\frac{df_1(x)}{dx} - f_1(x)\frac{df_2(x)}{dx}}{(f_2(x))^2}$$

19.) $$f_1(x) = \sqrt{R_S{}^2 + X_S{}^2}$$

20.) $$\frac{df_1(x)}{dx} = \frac{X_s}{(R_S^2 + X_S^2)^{1/2}}$$

21.) $$f_2(x) = \sqrt{(R_S + R_{Drive})^2 + (X_S + X_{Drive})^2}$$

22.) $$\frac{df_2(x)}{dx} = \frac{(X_S + X_{Drive})}{\sqrt{(R_S + R_{Drive})^2 + (X_S + X_{Drive})^2}}$$

Substituting eqs. 19, 20, 21, and 22 into 18 results in

23.)
$$\frac{d(\frac{|Z_S|}{|Z_T|})}{dx} = \frac{((R_S + R_{Drive})^2 + (X_S + X_{Drive})^2)^{1/2} \frac{X_s}{(R_S^2 + X_S^2)^{1/2}} - (R_S{}^2 + X_S{}^2)^{1/2} \frac{(X_S + X_{Drive})}{((R_S + R_{Drive})^2 + (X_S + X_{Drive})^2)^{1/2}}}{(R_S + R_{Drive})^2 + (X_S + X_{Drive})^2}$$

Multiplying top and bottom by $Z_T = ((R_S + R_{Drive})^2 + (X_S + X_{Drive})^2)^{1/2}$ and $Z_S = (R_S^2 + X_S^2)^{1/2}$ simplifies this expression to the following

24.) $$\frac{d(\frac{|Z_S|}{|Z_T|})}{dx} = \frac{X_S |Z_T|^2 - (X_S + X_{Drive})|Z_S|^2}{|Z_S||Z_T|^2}$$

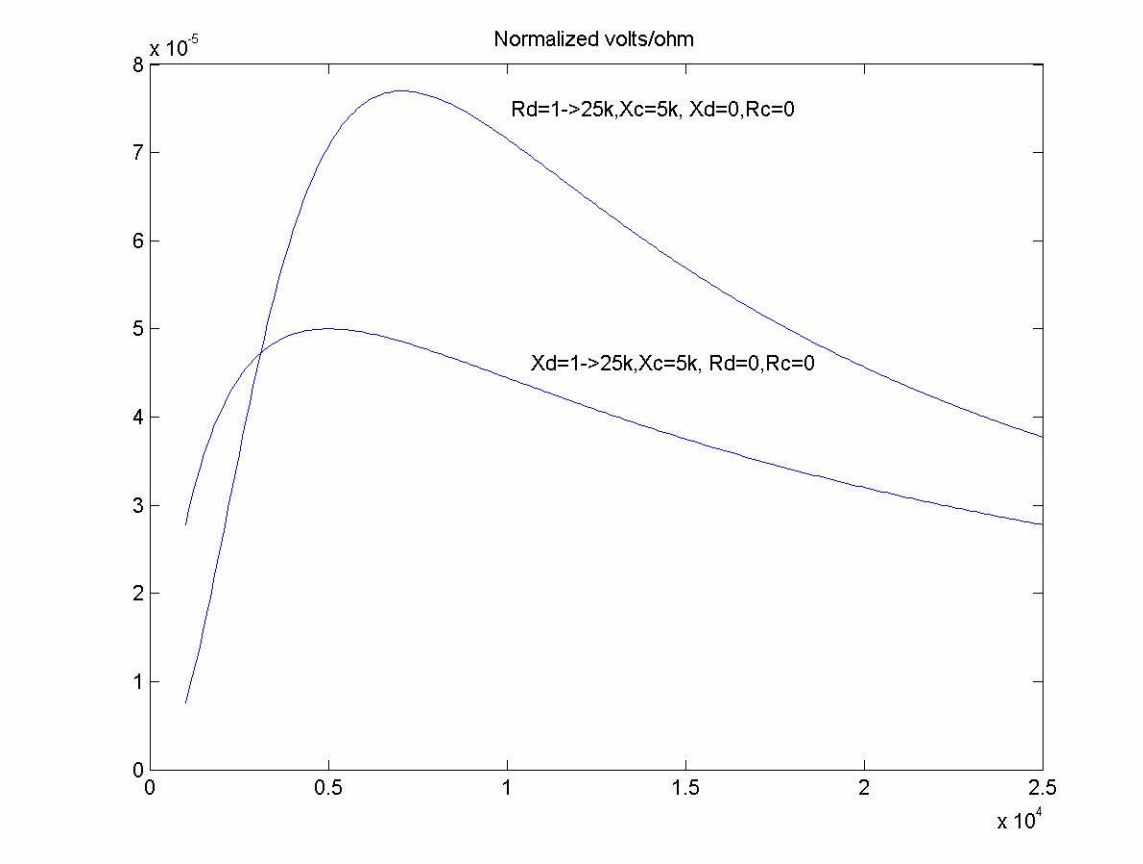

Fig. Two graphs for two different sets of capacitor and resistor values.

1.) $V_{Sensor} = I_{sensor} Z_{Sensor}$

2.) $Z_{Sensor} = R_s + iX_S$;

3.) $X_S = -i \dfrac{1}{2\pi f C_{Sensor}}$

4.) $Z_{Sensor} = |Z_S| e^{i\phi_S}$

5.) $|Z_S| = \sqrt{{R_S}^2 + {X_S}^2}$

6.) $\phi_S = \tan^{-1}\frac{X_S}{R_S}$

7.) $I_{Sensor} = \frac{V_{Drive}}{Z_{Total}}$

8.) $Z_{Total} = R_{Drive} + R_S + i(X_{Drive} + X_S)$

9.) $Z_{Total} = |Z_T|e^{i\phi_T}$

10.) $|Z_T| = \sqrt{(R_S + R_{Drive})^2 + (X_S + X_{Drive})^2}$

11.) $\phi_T = \tan^{-1}\frac{(X_S + X_{Drive})}{(R_S + R_{Drive})}$

12.) $V_{Sensor} = \frac{V_{Drive}}{Z_{Total}} Z_{Sensor}$

13.) $V_{Sensor} = \frac{V_{Drive}}{|Z_T|e^{i\phi_{Ti}}}|Z_S|e^{i\phi_S}$

14.) $V_{Sensor} = \frac{V_{Drive}}{|Z_T|}|Z_S|e^{i\phi_R}$

15.) $\phi_R = \phi_S - \phi_T$